THE JOURNAL OF PHYSICAL CHEMISTRY B

Article

pubs.acs.org/JPCB

Volume Transition and Adhesion Force of Nanosized Bifunctional Spherical Polyelectrolyte Brushes Observed by Dynamic Light Scattering and Atomic Force Microscopy

Shibin Huang,[†] Xuhong Guo,*[,†] Li Li,[†] and Yaming Dong*[,‡]

[†]State Key Laboratory of Chemical Engineering, East China University of Science and Technology, Shanghai 200237, PR China

[‡]Life and Environment Science College, Shanghai Normal University, Shanghai 200234, PR China

ABSTRACT: Stimuli-responsive nanoparticles have attracted considerable interest due to their enormous potential applications. In this paper, nanosized bifunctional spherical polyelectrolyte brushes (BSPBs) were prepared through grafting random copolymer chains from *N*-isopropylacrylamide (NIPA) and acrylic acid (AA) onto polystyrene core by photoemulsion polymerization. The pH- and thermo-responses of the BSPB with different ratio of NIPA and AA were investigated by dynamic light scattering. Atomic force microscopy (AFM) was employed to in situ monitor the pH response of the morphology and surface adhesion of BSPB as well as to visualize BSPB individually or as monolayer in air and liquid. The brush-like shell was illegible in electron microscopy images but clearly observed in AFM images. The results demonstrated that AFM was a powerful tool for in situ observing the stimulus-response of brushes on the surface of nanoparticles.

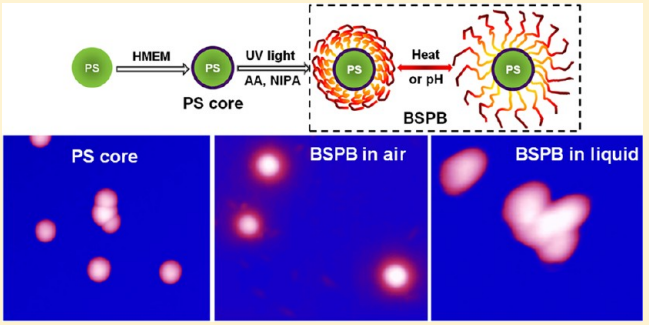

INTRODUCTION

Recently, there has been a great deal of concern over stimuli-responsive nanoparticles due to their fascinating tunable properties (e.g., size, shape and hydrophobicity) in response to external stimuli such as pH, temperature, light, etc. This class of nanoparticles has shown enormous application potentials in many fields involving drug delivery, biotechnology, sensor, membranes, catalysis, magnets and semiconducting materials.[1−7] Researchers attempted abundant ways to prepare functionalized smart polymer materials, including traditional emulsion polymerization, graft copolymerization, and core/shell microemulsion copolymerization.[8−10] Among them, colloidal technique for fabricating core−shell nanoparticles provides a facilitated path to obtain environment-responsive nanoparticles.[11−13]

Spherical polyelectrolyte (or polymer) brushes (SPBs) with high grafting density of poly(acrylic acid) (PAA) chains were sensitive to pH.[14] The PAA chains were chemically attached onto the colloidal polystyrene (PS) particle surface to form a brush-like shell (Figure 1) through photoemulsion polymerization. A significant transition could be found in the pH-titration curve of the brush thickness as determined by dynamic light scatter (DLS).[15,16] On the other hand, poly(*N*-isopropylacrylamide) (PNIPA), a famous thermo-sensitive polymer, was also grafted onto polymer core by a silimar method.[17−19] As it is well-known, PNIPA undergoes a marked volume phase transition around its lower critical solution temperature (LCST) in water. Owing to this characteristic, PNIPA microgels have been widely used as a targeted drug carrier for controlled drug release or "nanoreactors" for immobilized metal nanoparticles with selective catalysis.[20,21] The microgels consisiting of a copolymer of NIPA and AA displayed both pH dependence and thermo-sensitivity with a better hydrophilicity and site-specific function than PNIPA itself.[22]

To observe SPB, DLS, small-angle X-ray scattering (SAX), cryo-transmission electron microscopy (cryo-TEM) and second harmonic generation (SHG) were employed.[23−26] Among them, DLS provided the statistical and macroscopical information regarding particle size for the whole SPB suspension. However, as far as we know, a directly and in situ observation of nanosized SPB in liquid is still a challenge. It is difficult to discern brush layer from polymer core and to explore them in liquid environment by using common electron microscopy. However, atomic force microscopy (AFM) seems to be an ideal candidate to visually observe SPB and characterize their property in various conditions.[27] First of all, due to a high resolution image, AFM has been extensively used to study the subtle structure of architectural polymers such as combs, dendrigrafts, star polymers,[28−30] and SPBs.[31,32] Second, AFM can draw important information (such as height, friction, electrostatic force and magnetism) from samples as detected by a sensitive probe. Moreover, all AFM experimental operations were performed under common ambience without extreme vacuum. Last but not least, AFM can suffice as an observation of samples (e.g., biological specimens) in fluid.

Received: March 29, 2012
Revised: June 4, 2012
Published: July 26, 2012

   dx.doi.org/10.1021/jp302993t | *J. Phys. Chem. B* 2012, 116, 10079−10088

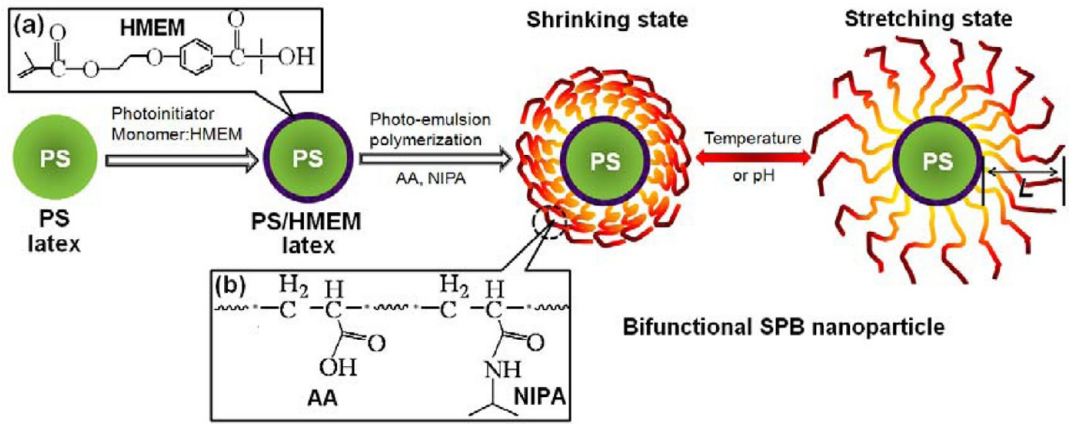

Figure 1. Schematic representation of the synthesis of pH- and thermo-responsive bifunctional spherical polyelectrolyte brushes of P (NIPA-*co*-PAA): (a) photoinitiator HMEM; (b) the shell of BSPB.

In this paper, nanosized bifunctional spherical polyelectrolyte brushes (BSPB) of P (NIPA-*co*-PAA) (Figure 1) with response to both pH and temperature were synthesized by photo-emulsion polymerization. DLS was utilized to macroscopically examine the double response of BSPB. AFM was employed to observe the morphology of BSPB individually or as monolayer in air and liquid. In particular, the pH response of morphology and surface adhesion force of BSPB was monitored in situ by AFM. To verify a volume transition induced by pH, AFM images of BSPB at different pH values were compared to observe the change of hydration state of brush layer with pH. Moreover, the surface adhesions of BSPB were determined at different pH values by force analysis of AFM.

Table 1. Recipe for Synthesis of Spherical Polymer Brushes

		cross-linker (g)	monomer (g)		
latex	PS (g)	BIS	AA	NIPA	AA/NIPA (mol/mol)
L_1	2.0	0.16	—	2.26	—
L_2	2.0	0.08	0.85	1.13	1.2:1
L_3	2.0	—	—	2.26	—
L_4	2.0	—	2.40	—	—
L_5	2.0	—	2.0	0.40	7.8:1
L_6	2.0	—	1.20	1.20	1.6:1

EXPERIMENTAL SECTION

Materials. *N*,*N*′-Methylenebis(acrylamide) (BIS; Fluka) and *N*-isopropylacrylamide (NIPA; Aldrich) were used as received. Sodium dodecyl sulfate (SDS), potassium peroxodisulfate (KPS), sodium hydrogen sulfite (SHS), nickel acetate were purchased from Shanghai Lingfeng Chemical reagent Co., LTD and used as received. Styrene (Shanghai, Lingfeng) and acrylic acid (AA) (Shanghai, Lingfeng) were distilled under reduced pressure to remove the inhibitor and stored in the refrigerator before use. The photoinitiator 2-[p-(2-hydroxy-2-methylpropiophenone)]-ethylene glycol-methacrylate (HMEM) was synthesized according to our previous publication.[14] All water used in this study was purified with a Millipore Milli-Q system, and the resistivity was above 18 MΩ cm.

An atomical flatness mica (Shanghai NTI Co.) served as the substrate for directly deposition of BSPB by conveniently cleaving, which was cut with a square of 10 × 10 mm. It was also further treated with multivalent cation to facilitate anchoring anionic BSPB in liquid. Typically the nickel acetate aqueous solution (0.01M) was dropped onto a freshly cleaved mica surface and dried in air, then rinsed with water.

Synthesis of BSPB. BSPBs were prepared in two steps. In the first step, PS core latex grafting with a thin layer of photoinitiator HMEM was synthesized. Typically 20.0 g of styrene, 550 g of H_2O, and 0.40 g of SDS were charged into 1000 mL three-neck round-bottom flask equipped with

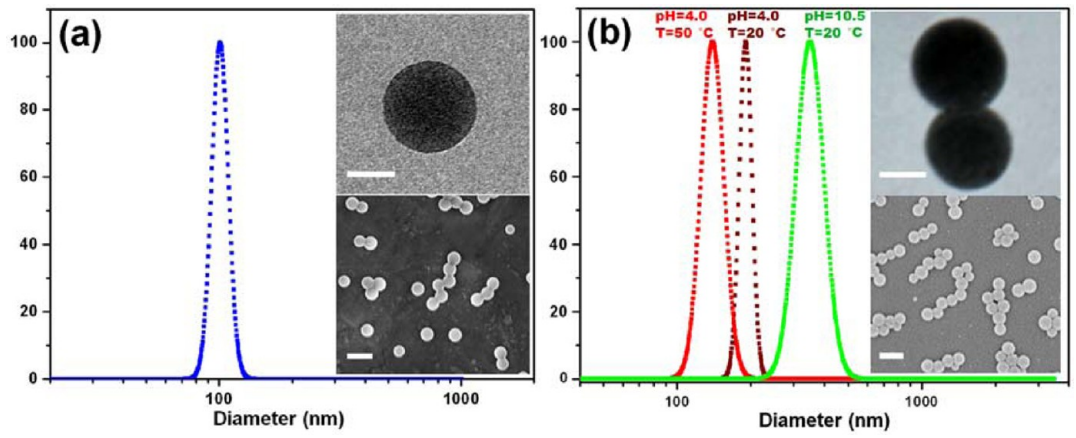

Figure 2. Size and size distribution of PS core (a) and BSPB (L_2) (b) observed by DLS, TEM, and SEM. The insets are TEM (upper) images with a scale bar of 50 nm and SEM (down) images with a scale bar of 200 nm.

dx.doi.org/10.1021/jp302993t | *J. Phys. Chem. B* 2012, 116, 10079−10088

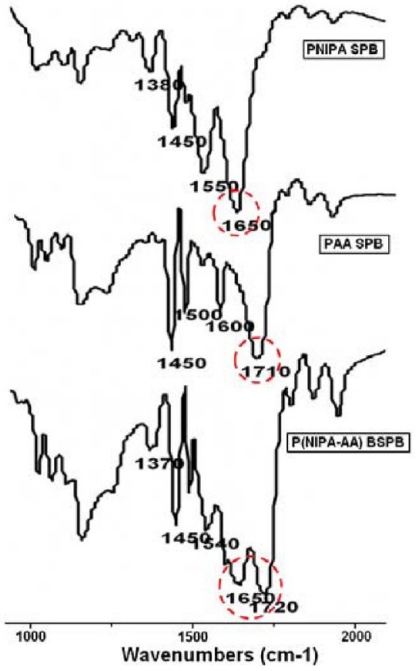

Figure 3. FTIR spectra of PNIPA SPB (L_3), PAA SPB (L_4) and BSPB (L_5).

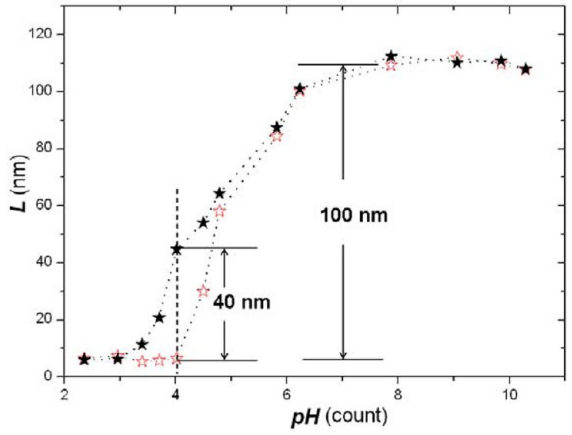

Figure 4. Thickness L of BSPB (L_2 in Table 1) as a function of pH. The changing parameter is temperature. The BSPB exhibited thermosensitivity as well as pH-sensitivity at pH value from 3 to 6. Key: (★) 23 °C; (☆) 55 °C.

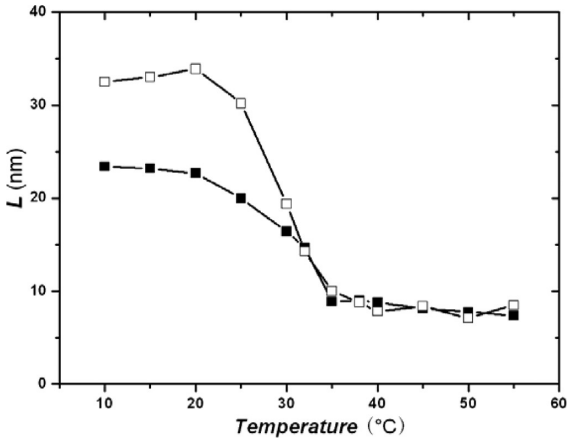

Figure 5. Thickness of brush layer as a function of temperature for spherical PNIPA brush (L_1) and BSPB (L_2) at pH of 5. Key: (■) L_1 and (□) L_2.

mechanical stirrer at the temperature of 35 °C. Polymerization was carried out by adding of 0.350 g of KPS and 0.28 g of SHS as initiators. The reaction lasted for 1 h. Subsequently, HMEM solution (2.0 g HMEM was dissolved in 5 mL of acetone) was added dropwise into reaction system at a rate of 3 mL/h. After the last addition the reaction mixture was stirred for 1 h. The whole process was kept at 35 °C. The obtained latexes were cleaned by ultrafiltration.

In the second step, BSPB were prepared by photoemulsion polymerization. In a typical run, 500 g of the as-prepared PS core latexes with the concentration of 0.4 wt % were charged into a home-built UV-reactor (range of wavelengths, 200−600 nm; power, 150 W). Then monomers (as shown in Table 1) were added under stirring. Usually NIPA monomer was added at first to react for 20 min at 45 °C under exposure of UV light, and then AA was added. The polymerization was triggered by UV irradiation with range of wavelengths of 200−600 nm under the protection of nitrogen gas and totally lasted for 2 h. The products were purified exhaustively by serum replacement until the conductance of the eluate did not change anymore.

Fourier Transform Infrared Spectroscopy (FT-IR). The FTIR spectra of the dried core shell particles were taken in KBr pellet using Nicolet 6700 spectrometer instrument (Thermo Fisher Scientific Inc., USA). The spectra were recorded at room temperature and background-corrected.

Electron Microscopy. The sample was observed by field emission scanning electron microscope (FE-SEM) (Hitachi JSM-6360LV) equipped with an energy-dispersive X-ray (EDX) detector at an electron acceleration voltage of 15 kV. The sample was prepared by dilution of latex with Milli-Q water to concentration of 0.05 wt %, and then deposited suspension onto fresh cleaved mica for air drying.

Morphology of the samples was also characterized using transmission electron microscopy (JEOL 100CX at 100 kV, Japan) (TEM). A Formvar-coated copper grid was dip coated with sample latex suspension and dried under the irradiation of infrared lamp.

Dynamic Light Scattering (DLS). Particle size was determined at different temperatures by using a NICOMP 380 ZLS light scattering goniometer (Particle Sizing Systems, USA) at a scattering angle of 90°. Samples were prepared with different pH values and constant salt concentration, which were adjusted by aqueous HCl, NaOH, and NaCl solutions. The pH was measured with a Crison (GLP 21) pH meter. The thickness of brush layer was calculated from the hydrodynamic radius of SPB and core as determined by DLS.

Atomic Force Microscopy. All the AFM observations were performed in air or fluid at 26 ± 1 °C under tapping mode operation with a Multimode Nanoscope IIIa unit (Vecco Metrology Group, now Bruker AXS). In air imaging, 10 μL of the diluted BSPB suspensions (volume ratio of 1:50 of BSPB latex and water) with a pH of 7.1 and 10.2 were pipetted onto freshly cleaved mica surface respectively, and then dried at 5 °C in refrigerator before observation. A NP-S silicon cantilever (0.58 N/m, 349 ± 1 Hz, Veeco Metrology Group, now Bruker AXS) was used here for tapping mode AFM (TPAFM) scanning. To minimize the squeezing between tip

dx.doi.org/10.1021/jp302993t | J. Phys. Chem. B 2012, 116, 10079−10088

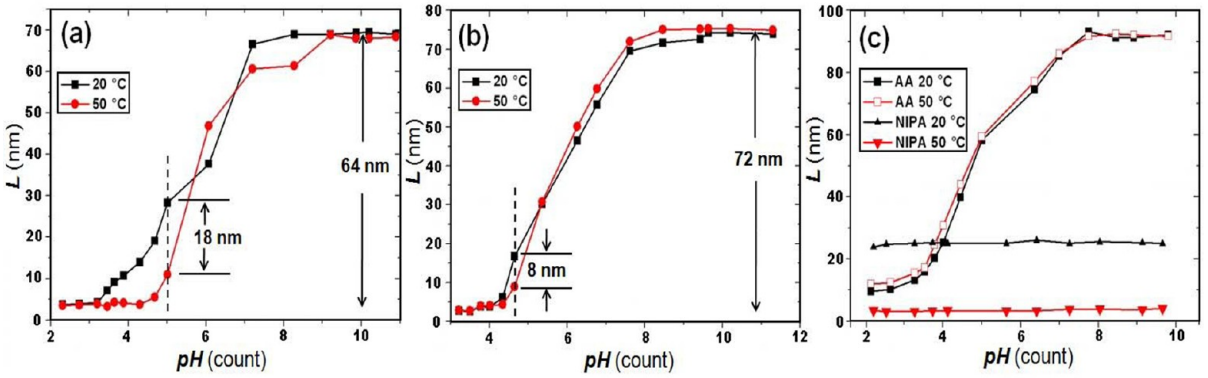

Figure 6. Thickness of brush as a function of pH. The changing parameter is temperature: (a) $\mathbf{L}_6$ with a mole ratio of AA and NIPA of 1.6:1; (b) $\mathbf{L}_5$ with a mole ratio of AA and NIPA of 7.8:1; (c) PAA ($\mathbf{L}_4$) and PNIPA brush ($\mathbf{L}_3$).

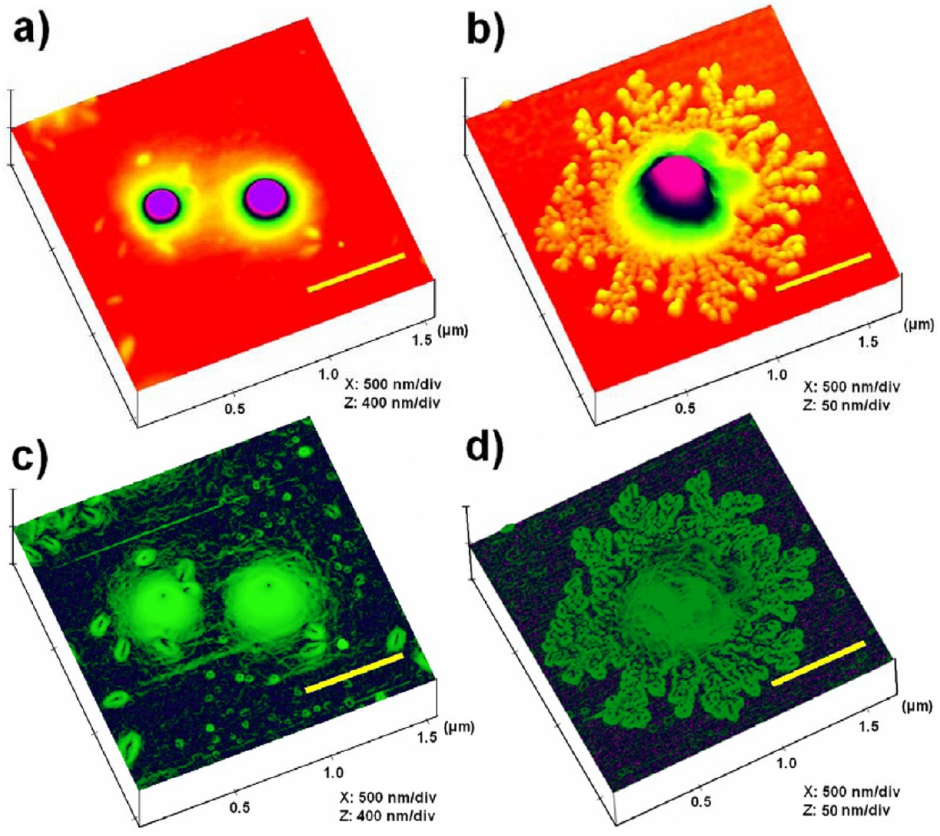

Figure 7. Three-dimensional images of BSPB ($\mathbf{L}_6$) supported on mica obtained by air scanning of AFM. BSPB suspensions with pH of 7.1 (a, c) and 10.2 (b, d) were deposited for AFM observing. The "height" mode (a, b) and the "illuminate" mode (c, d) were different treatments of AFM offline software for the same image. The scale bars are 500 nm.

and brush, the distance between tip and sample in the scanning was controlled by force-curve analysis.

In fluid imaging, the BSPB particles were anchored to Ni^{2+}-modified mica surface (N-MS) by an electrostatic attraction force. The deposition process of BSPB involves three cases: (1) incubating of N-MS in anionic BSPB latex (0.05 wt %) for a mimimum of 20 min immediately followed by flushing with water; (2) spin-coating of diluted BSPB suspension (0.5 wt %) upon N-MS; (3) adding two drops of diluted suspension (0.5 wt %) on N-MS and drying at room temperature. After each process above, the samples were flushed with water adequately to wash unadsorbed nanoparticles, and eventually dried under ambient conditions at temperature of 26 ± 1 °C. NP-10 triangular silicon nitride probe (0.24 N/m, Veeco Metrology Group, now Bruker AXS) and a fluid cell were employed for fluid tapping mode imaging. Here a fast scan rate was carried out within 2.0 to 4.0 Hz.

Force analysis was performed in fluid with a real time observation. The aqueous solutions with pH of 3.0, 6.5, and 9.0 were injected into fluid cell by syringe, respectively. In order to eliminate the effect of temperature, the measurement system was equilibrated for 20 min after each change of solution. The scan rate of Z orientation was controlled as a range from 0.5 to 1.0 Hz to minimize cumulative effects, which might resulted

dx.doi.org/10.1021/jp302993t | J. Phys. Chem. B 2012, 116, 10079−10088

from hysteresis of properties of polymer shells during a repeatedly compressed process. Approximately 20 extension/retraction cycles were performed at each pH.

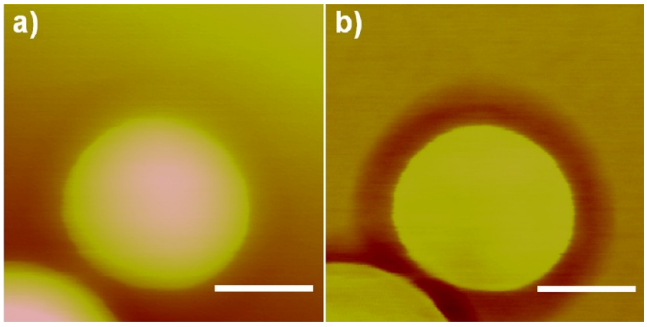

Figure 8. AFM images of cross-linked PNIPA SPBs (L_1) on mica surface: (a) height image; (b) phase contrast image. The scale bars are 50 nm.

RESULTS AND DISCUSSION

Synthesis of Bifunctional Spherical Polyelectrolyte Brush. In the first step of BSPB preparation, narrowly dispersed polystyrene core latexes grafting a thin layer of initiator were synthesized by controlled emulsion polymerization. During the process of adding initiator HMEM, it should be emphasized that the polymerizable HMEM should be charged very slowly into reactive medium under a "starved condition" at the last stage of emulsion polymerization of styrene. Here a cautious feeding of initiator was for the aim that each precusor colloidal particle has an equal opportunity to gain HMEM monomers. Thus, HMEM was homogeneously covered onto PS cores covalently by copolymerization with remained styrenes leading to formation of well-defined spherical brushes. As one can see in Figure 2a, the DLS data indicated that the PS core nanoparticles were ca. 100 nm in diameter with a narrow size distribution. The SEM and TEM

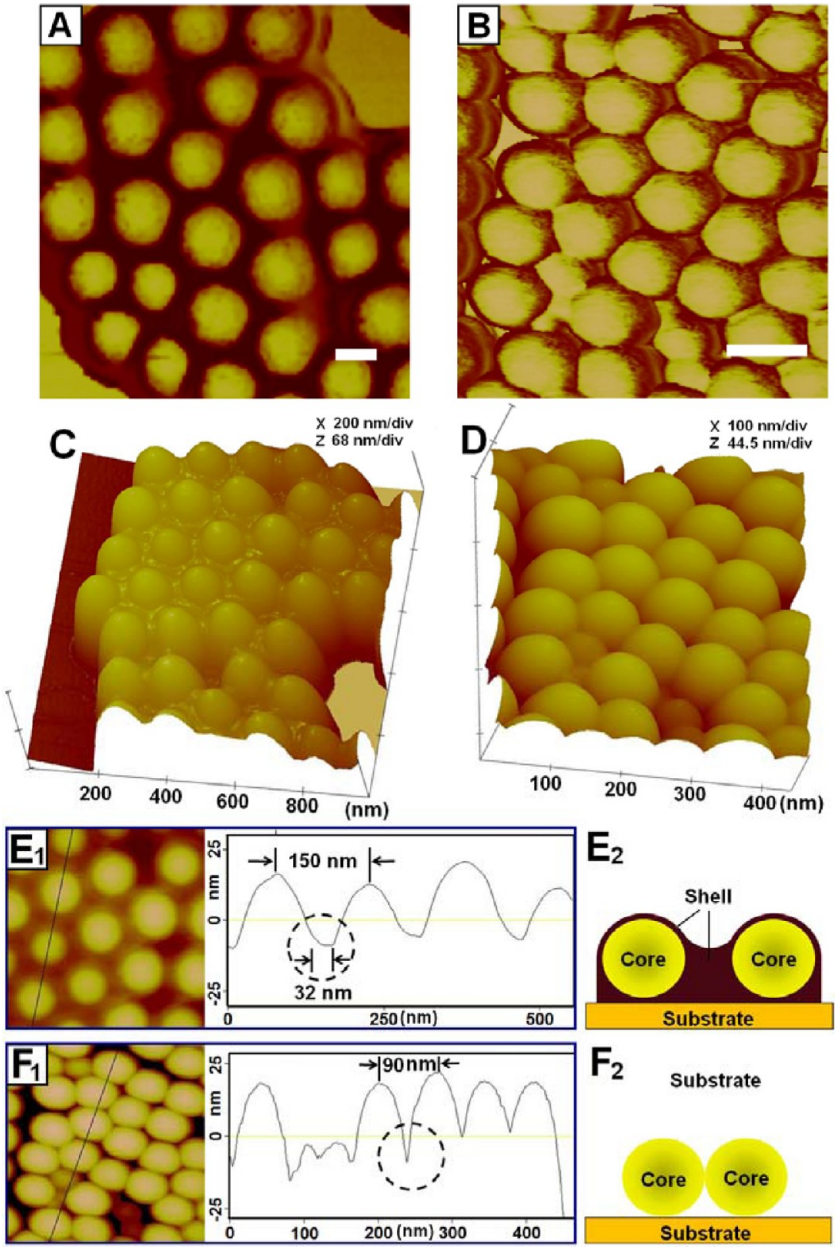

Figure 9. AFM images of BSPBs (L_6) (A, C, E) and PS cores (B, D, F) self-assembled on mica surface. Phase images (A, B), three-dimensional images (C, D), cross section analysis (E_1, F_1), and schematic diagrams (E_2, F_2) of BSPBs and PS cores. The scale bars are 100 nm.

dx.doi.org/10.1021/jp302993t | J. Phys. Chem. B 2012, 116, 10079−10088

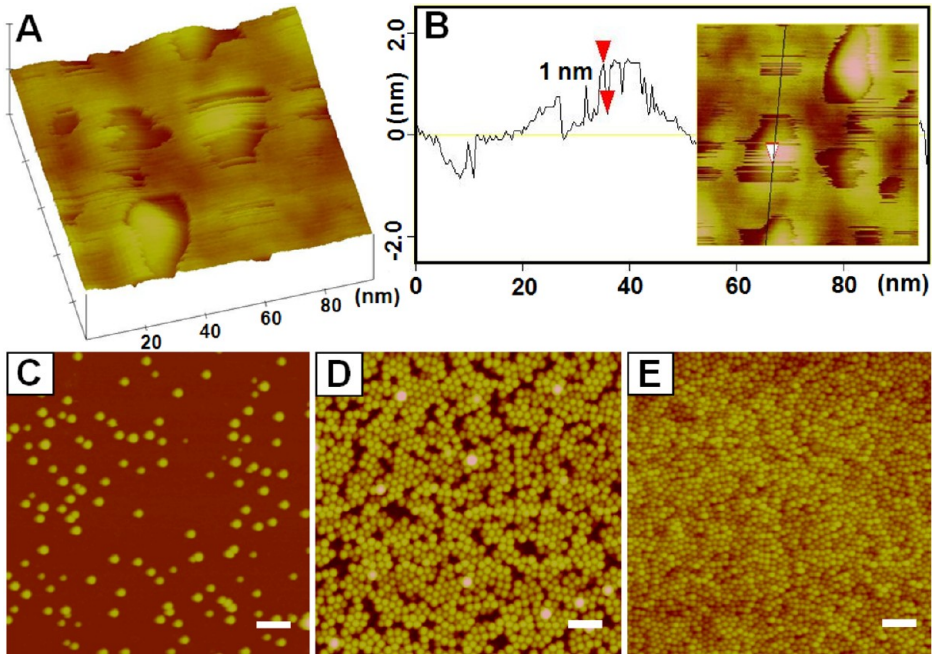

Figure 10. AFM height images of BSPBs ($\mathbf{L}_6$) self-assembled on mica surface modified by nickel salt. (A) Three-dimensional height image of nickel salt layer. (B) Section analysis of part A. (C–E) Self-assemblies of BSPBs on N-MS by dipping, spin-casting, and excessive deposition, respectively. The scale bars are 500 nm.

images (see the insets in Figure 2a) confirmed the homogeneously spherical shape of the as-prepared PS cores.

In the second step, BSPB were grown on the PS core. In order to guarantee the formation of well-defined shell, the reaction temperature of photoemulsion polymerization (45 °C) was above the LCST of PNIPA (32 °C).[19] The copolymerization of NIPA and AA was triggered by photolysis of HMEM. To verify the grafting of two functional units, a comparison of FTIR spectra of PNIPA SPB, PAA SPB and BSPB was presented in Figure 3. The two peaks at around 1650 and 1710 cm^{-1} which were used to identify carboxyl and amide groups respectively, were clearly presented in the spectrum of BSPB. It reflects the fact that both NIPA and AA units were grafted on the PS core successfully.

In Figure 2, the thickness of BSPB layers grafted on latex $\mathbf{L}_2$ (Table 1) was ca. 125 nm at pH = 10.5 and 20 °C, which was deduced by subtraction of a diameter of PS core (100 nm) from that of BSPB (350 nm). As pH decreased from 10.5 to 4.0 at 20 °C, the thickness decreased from 125 to 45.5 nm. When the temperature increased to 50 °C beyond the LCST of PNIPA, the thickness of BSPB further reduced from 45.5 to 16.5 nm, which confirmed again that both NIPA and AA units were grafted onto PS core surface.

Thermal and pH Response Observed by DLS. Figure 4 showed the thickness (L) of BSPB measured by DLS as a function of the pH value of suspension. A marked volume transition from pH 3 to 8 during titration confirmed that the BSPB showed pH responsibility like PAA brush. Moreover, as one can see in the dashed line, the deviation of two curves at 23 and 55 °C indicated the thermal response of BSPB. The BSPB thickness at 55 °C was obviously smaller than that at 23 °C from pH 3 to 6. The maximum difference of two curves appeared at pH = 4. It seems that the thermal responsibility of BSPB was more significant at a low pH (pH < 5) where most of the carboxy groups of PAA were un-ionized, while the pH responsibility became dominant when pH > 5. Moreover, the onset of the volume transition shifted to high pH value upon increasing temperature (Figure 4).

As showed in Figuer 5, BSPB showed the similar thermal response with PNIPA SPB ($\mathbf{L}_1$) at pH = 5, although with a different thickness level. This phenomenon revealed that the existing of AA units in BSPB did not change the thermo-reponsive region of brush.

In order to investigate the effect of the ratio of two functional monomers on double responsibility, $\mathbf{L}_6$ with a mole ratio of AA and NIPA of 1.6:1 and $\mathbf{L}_5$ with a mole ratio of 7.8:1 were both titrated (Figure 6 a and b). $\mathbf{L}_6$ with more NIPA units showed a more significant thermo-responsibility compared to $\mathbf{L}_5$. As expected, the PNIPA brushes are pH independent while PAA brushes have no thermal responsibility (Figure 6c). Therefore, the thermo- and pH-responsibility can be tuned by the ratio of NIPA and AA.

Morphology Observation by AFM in Air. The dry spherical brushes can hardly be "seen" by means of common electronic microscopy due to the collapse and possible degradation of brush polymer chains under the electron flow with high energy (Figure 2). In this work, AFM was employed to observe BSPB in air and fluid, respectively. The height, phase, and illuminate modes were adopted in our experiment to show the configuration of BSPB. The height image mainly shows the height variations of sample surface, while the phase image maps the distribution of physical or chemical properties. Illuminate is a model for three-dimensional image with a light source from a selected direction. Considering the soft and delicate brush layers, topographical mapping of BSPBs on substrates were performed under tapping mode, in which the cantilever was excited into resonance oscillation by a piezoelectric driver, and thus the interaction between the tip and the surface was in the contact and noncontact region intermittently. The observation benefited from this tapping mode due to a minimum squeeze and damage loaded on sample during the tip's scanning.

dx.doi.org/10.1021/jp302993t | J. Phys. Chem. B 2012, 116, 10079–10088

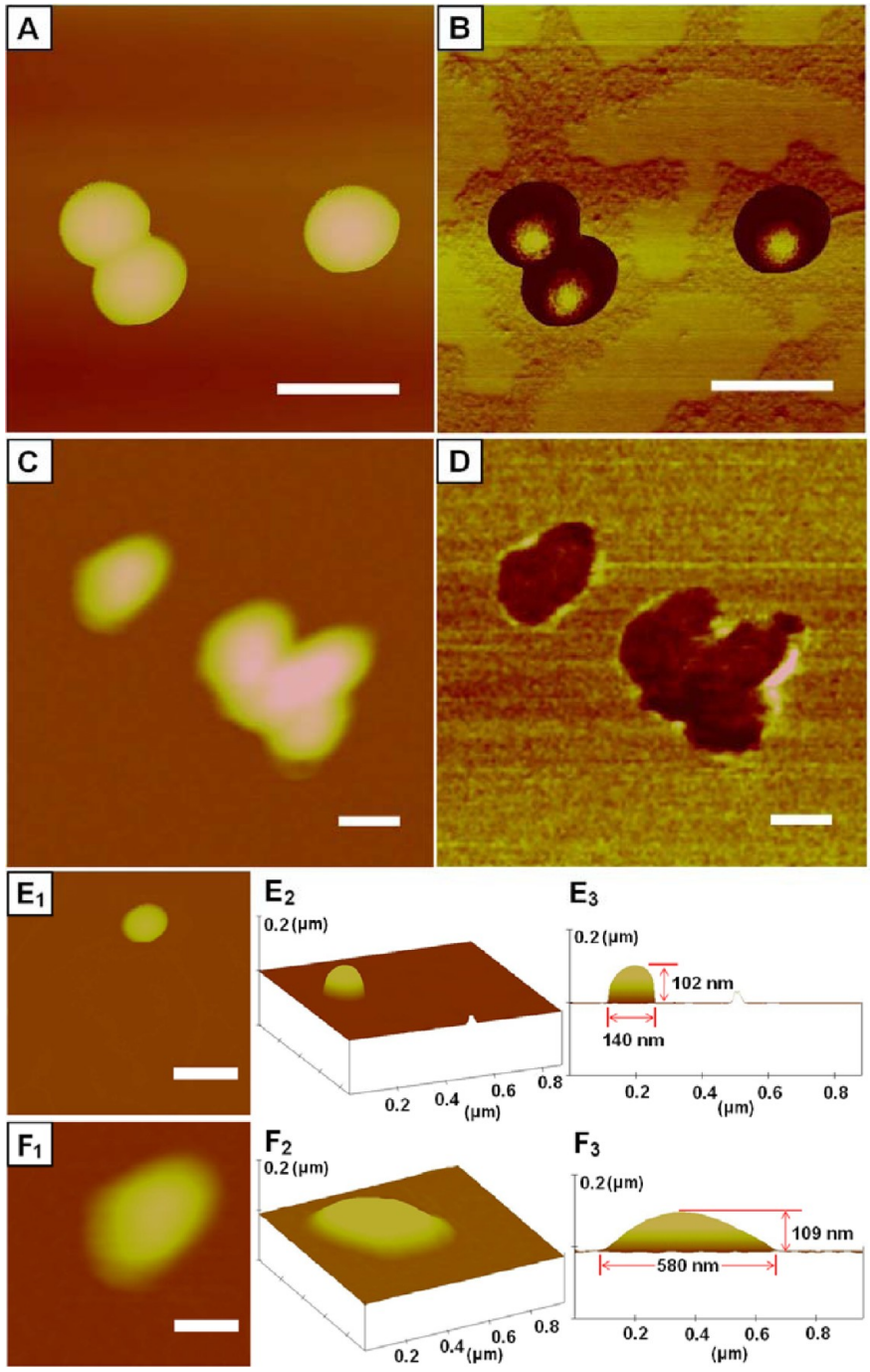

Figure 11. AFM observations of BSPB ($\mathbf{L_6}$) in air (A, B and E) and fluid (C, D, and F). B and D are phase images; the others are topographic ones (E_2, E_3, F_2, F_3 are 3D images). The scale bars are 200 nm.

The dried BSPBs from neutral and basic suspensions showed different morphologies on mica surface (Figure 7). The "height" (Figure 7, parts a and b) and "illustrate" (Figure 7, parts c and d) images were employed to analyze the morphology of brushes, which were obtained from 3D image analysis by AFM off-line software. As shown in Figure 7a, a corona around a spherical core as a typical feature of BSPB under a neutral deposition can be observed. The color corresponds to the height in topographic image. Two neighboring BSPBs were separated while slightly overlapped due to a weakly repulsive interaction (Figure 7c). For BSPB prepared by a suspension with pH = 10.2 (Figure 7, parts b and d), a dendritic structure was found around the core which seemed to be aggregation induced by brush chains when drying.

It is worth to note that the brush chains usually collapse to core surface after drying while the BSPB chains spread on mica surface due to the strong interactions with highly hydrophilic mica surface. In order to see a more stable brush shell under AFM, PNIPA SPBs were cross-linked by BIS and observed under TPAFM in air (Figure 8). In phase image (Figure 8b), a satisfied contrast between cross-linked shell and core was obtained. Indeed, we can see the brush clearly by means of AFM.

Self-assembled monolayer of BSPB was also observed under AFM (Figure 9). In Figure 9A, a sharp contrast between brush layer and PS core was given by phase images, and thus the brush layers and PS cores were able to be distinguished easily in

dx.doi.org/10.1021/jp302993t | J. Phys. Chem. B 2012, 116, 10079−10088

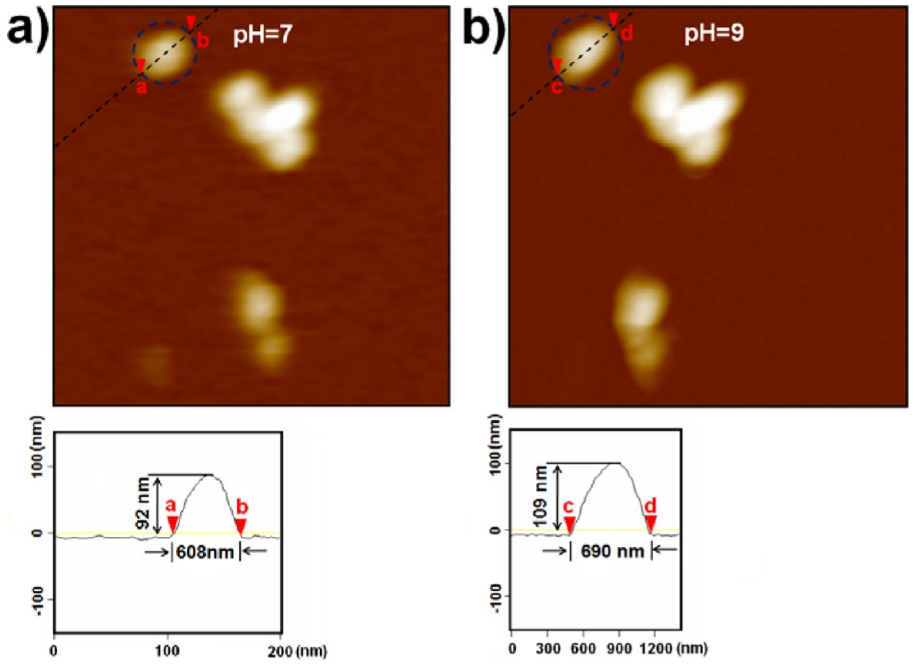

Figure 12. AFM height images of BSPBs (L_6) in situ obtained in aqueous solution of pH 7 and 9.

color contrast. This contrast originated from the difference in surface properties between brush shell and PS core which led to different phase lags as the oscillating probe scaned across them. Since the BSPB brush layer is hydrophilic, the absorbed water can also enhance the contrast between the brush and the hydrophobic PS core. The oscillation amplitude was used as a feedback signal to measure topographic variations of the sample, and the phase lag was simultaneously measured with amplitude for generating phase images. When the tip contacts the objects, the amplitude of the oscillation will be declined and the phase will be laged behind the drive signal. The phase lag is usually sensitive to the variation of composition, adhesion, friction, and viscoelasticity etc. Thus, the phase imaging can map the surface property.

Moreover, the difference between BSPB and PS core could be distinguished by section analysis of BSPB and PS core. The junction of BSPBs was flat (Figure $9E_1$), whereas a sharp valley appeared between PS cores (Figure $9F_1$). These pictures were schematically represented in Figure $9E_2$ and F_2. The distance of two BSPBs (150 nm) was larger than that of PS cores (90 nm), which also reflected the existence of brush layer between two neighboring BSPBs.

Morphology Observation by AFM in Fluid. Having observed BSPB in air, we turn to "see" them in aqueous solution by AFM. Before observation, the anionic BSPB were anchored on the mica surface with the assistance of divalent Nickel cations. A layer of nickel salt with one nanometer thickness was deposited on freshly cleaved mica surface (Figure 10, parts A and B). The patches on the nickel salt layer were probably resulted from scratching of extremely sharp tip when scanning with relatively large amplitude. BSPBs self-assembled on Ni^{2+}-modified mica surface (N-MS) by dipping, spin-casting and excessive deposition were displayed in Figure 10, parts C−E, respectively.

When BSPBs were dispersed in aqueous solution, the brush layers hydrated and expanded compared to those in air, and thus prevented the AFM tip from touching the PS core (Figure 11). Therefore, in phase images, the core of BSPB was visualized in air imaging (Figure 11B) whereas invisible in fluid imaging (Figure 11D). Compared to the collapsed brush layer in air (Figure $11E_{1-3}$), BSPB showed a highly swollen shell in liquid (Figure $11F_{1-3}$). It should be noted that the BSPB looked like a flat spherical cap in liquid (Figure $11F_3$) due to the strong attraction between brush chains and subtracte.

PH Response Observed by AFM in fluid. The change in volume of BSPB induced by pH was observed under AFM in situ in fluid (Figure 12). The BSPB layer adsorbed on N-MS was enclosed in a fluid cell sealed by a silicon O-ring and observed by AFM. We changed the solution in fluid cell with a syringe very carefully in order to minimize the movement of BSPBs. To find the same objects again, the probe was lifted not too far from the mica surface (e.g., tens micrometers). Upon changing the pH from 7 to 9, the volume of BSPB deposited on N-MS expanded (Figure 12) due to the extending of brush chains caused by increased electrostatic repulsion force. The section analyses also showed the change in shape (height and width) of coronal-like BSPB particle upon changing pH value.

To further insight the pH-response of BSPB, AFM force analysis was employed to estimate qualitatively the adhesion of BSPB monolayer at various pH values (Figure 13). A monolayer comprised of close-packed BSPBs on N-MS (Figure 10E) was observed by AFM in fluid. No attraction force to the silicon nitride tip was found at pH of 3.0 (Figure $13a_3$). Upon increasing pH, the attraction force to the tip increased significantly. It means that the adhesion between BSPB shell and silicon nitride tip was turnable by pH. The adhesion of BSPB was due to the dissociation of carboxyl group in PAA. In order to avoid the impact of temperature on the measurement, the system reached equilibrium by waiting at least for 20 min after injecting solution to adjust the pH. All the AFM operations were carried out at temperature of 26 ± 1 °C. Moreover, prior to a force curve analysis, a homogeneous and clean target zone without defect and contamination which might cause a deviation of force measurement was chosen.

dx.doi.org/10.1021/jp302993t | J. Phys. Chem. B 2012, 116, 10079−10088

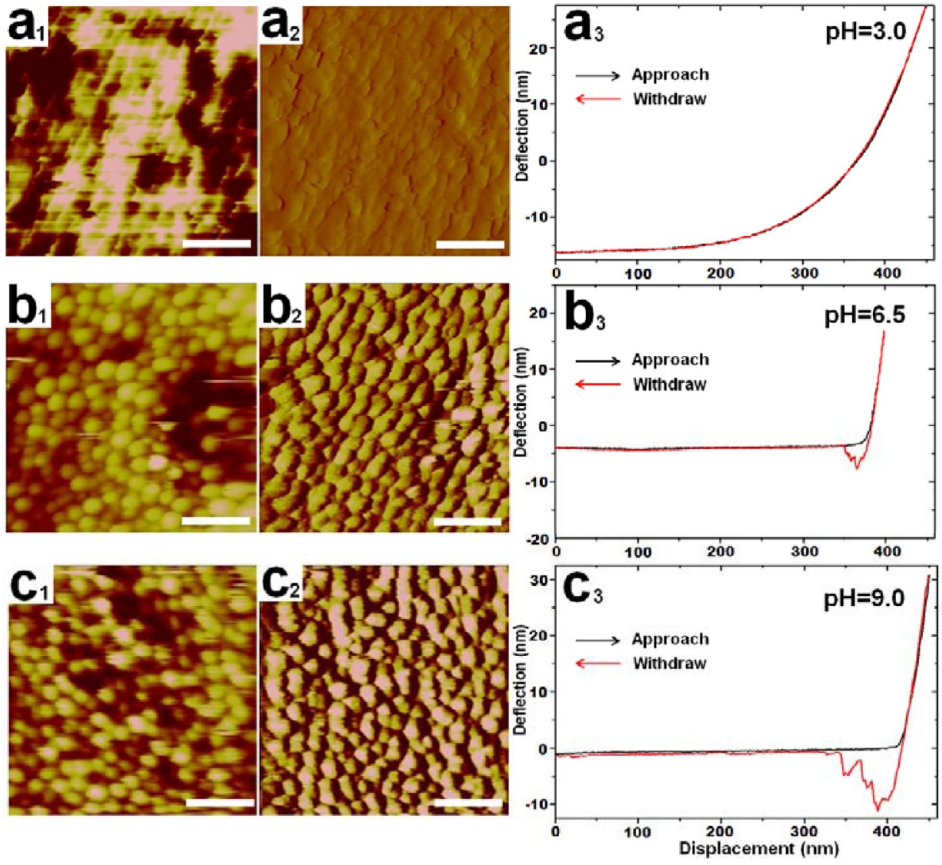

Figure 13. AFM images and the corresponding force-curves of BSPB (L_6) monolayer obtained in solutions of pH 3.0 (a_{1-3}), 6.5 (b_{1-3}) and 9.0 (c_{1-3}). Here, a_1, b_1 and c_1 are the height images, while a_2, b_2, c_2 are the phase images. Scale bar =500 nm.

CONCLUSION

Well-defined bifunctional spherical polyelectrolyte brushes (BSPB) were successfully synthesized by photoemulsion polymerization of NIPA and AA. The BSPB exhibited both pH- and thermo-sensitivity, which was tunable by altering the ratio of NIPA and AA. The volume transition upon changing pH and temperature obtained from DLS confirmed the double responses of BSPB. Both the brush layer and the core were visible in air and fluid by AFM, while the pH response of brush could be observed in situ in fluid by AFM. The surface adhesion of BSPB to AFM tip increased upon increasing pH. AFM was demonstrated to be a powerful tool to see the change of morphology and surface adhesion of BSPB. This work opened up a new way to in situ observe the surface behavior of brushes or nanoparticles in solution.

AUTHOR INFORMATION

Corresponding Author

*Telephone/Fax: +86 21 6425 3491. E-mail: guoxuhong@ecust.edu.cn (X.G.); ymdong@shnu.edu.cn (Y.D.).

Notes

The authors declare no competing financial interest.

ACKNOWLEDGMENTS

We gratefully acknowledge the National Natural Science Foundation of China (Grant No. 20774028 and 11076002/A06), the Fundamental Research Funds for the Central Universities, the higher school specialized research fund for the doctoral program (20110074110003), and the Key Basic Research Project of Shanghai Science and Technology Commission (10JC1403800) for support of this work.

REFERENCES

(1) Das, M.; Mardyani, S.; Chan, W. C.; W.; Kumacheva, E. *Adv. Mater.* **2006**, *18*, 80−83.
(2) Ali, M. M.; Su, S.; Filipe, C. D. M.; Pelton, R.; Li, Y. *Chem. Commun.* **2007**, *43*, 4459−4461.
(3) Hendrickson, G. R.; Lyon, L. A. *Soft Matter* **2009**, *5*, 29−35.
(4) Ulbricht, M. *J. Chromatogr. B* **2004**, *804*, 113−125.
(5) Zhang, M. C.; Zhang, W. Q. *J. Phys. Chem. C* **2008**, *112*, 6245−6252.
(6) Pich, A.; Bhattacharya, S.; Lu, Y.; Boyko, V.; Adler, H. A. P. *Langmuir* **2004**, *20*, 10706−10711.
(7) Zhang, J. G.; Xu, S. Q.; Kumacheva, E. *J. Am. Chem. Soc.* **2004**, *126*, 7908−7914.
(8) Cernakova, L'U.; Chrastovae, V.; Volfova, P. *J. Macromol. Sci. A* **2005**, *42*, 427−439.
(9) Gu, S.; Wang, Y.; Zhang, F. *J. Macromol. Sci. A* **2005**, *42*, 771−781.
(10) Zhang, Y.; Guo, T.; Hao, G.; Song, M.; Zhang, B. *Int. J. Polym. Mater.* **2005**, *54*, 279−291.
(11) Berndt, I.; Pedersen, J. S.; Richtering, W. *Angew. Chem., Int. Ed.* **2006**, *45*, 1737 −1741.
(12) Jones, C. D.; Lyon, L. A. *Macromolecules* **2003**, *36*, 1988−1993.
(13) Bradley, M.; Vincent, B. *Langmuir* **2008**, *24*, 2421−2425.
(14) Guo, X.; Weiss, A.; Ballauff, M. *Macromolecules* **1999**, *32*, 6043−6046.
(15) Guo, X.; Ballauff, M. *Phys. Rev. C* **2001**, *64*, 051406.
(16) Guo, X.; Ballauff, M. *Langmuir* **2000**, *16*, 8719−8726.
(17) Lu, Y.; Wittemann, A.; Ballauff, M.; Drechsler, M. *Macromol. Rapid Commun.* **2006**, *27*, 1137−1141.

(18) Hoffmann, M.; Siebenbürger, M.; Harnau, L.; Hund, M.; Hanske, C.; Lu, Y.; Wagner, C. S.; Drechsler, M.; Ballauff, M. *Soft Mater* **2010**, *6*, 1125−1128.
(19) Wang, X.; Guo, X.; Zhu, Y.; Li, L.; Wu, S.; Zhang, R. *Chin. J. Polym. Sci.* **2011**, *29*, 490−496.
(20) Oh, J. K.; Drumright, R.; Siegwart, D. J.; Matyjaszewski, K. *Prog. Polym. Sci.* **2008**, *33*, 448−477.
(21) Wu, S.; Dzubiella, J.; Kaiser, J.; Drechsler, M.; Guo, X.; Ballauff, M.; Lu, Y. *Angew. Chem., Int. Ed.* **2012**, *51*, 2229−2233.
(22) Jones, C. D.; Lyon, L. A. *Macromolecules* **2000**, *33*, 8301−8306.
(23) Dingenouts, N.; Norhausen, Ch.; Ballauff, M. *Macromolecules* **1998**, *31*, 8912−8917.
(24) Crassous, J.; Rochette, C.; Wittemann, A.; Schrinner, M.; Ballauff, M. *Langmuir* **2009**, *25*, 7862−7871.
(25) Bolisetty, S.; Schneider, C.; Polzer, F.; Ballauff, M. *Macromolecules* **2009**, *42*, 7122−7128.
(26) Schürer, B.; Hoffmann, M.; Wunderlich, S.; Harnau, L.; Peschel, U.; Ballauff, M.; Peukert, W. *J. Phys. Chem. C* **2011**, *115*, 18302−18309.
(27) Huang, S.; Guo, X.; Li, L.; Xu, H.; Dong, Y. *Appl. Mech. Mater.* **2011**, *110*−*116*, 3762−3769.
(28) Deffieux, A.; Schappacher, M.; Hirao, A.; Watanabe, T. *J. Am. Chem. Soc.* **2008**, *130*, 5670−5672.
(29) Matyjaszewski, K.; Qin, S.; Boyce, J. R.; Shirvayants, D.; Seiko, S. S. *Macromolecules* **2003**, *36*, 1843−1849.
(30) Seiko, S. S.; Da Silva, M.; Shirvayants, D.; LaRue, I.; Prokhorova, S.; Möller, M.; Beers, K.; Matyjaszewski, K. *J. Am. Chem. Soc.* **2003**, *125*, 6725−6728.
(31) Mei, Y.; Wittemann, A.; Sharma, G.; Ballauff, M. *Macromolecules* **2003**, *36*, 3452−3456.
(32) Gliemann, H.; Mei, Y.; Ballauff, M.; Schimmel, T. *Langmuir* **2006**, *22*, 7254−7259.